

# High-Frequency Variability in the Circulation and Hydrography of the Denmark Strait Overflow from a High-Resolution Numerical Model<sup>✉</sup>

MATTIA ALMANSI AND THOMAS W. N. HAINE

*Department of Earth and Planetary Sciences, The Johns Hopkins University, Baltimore, Maryland*

ROBERT S. PICKART

*Woods Hole Oceanographic Institution, Woods Hole, Massachusetts*

MARCELLO G. MAGALDI

*Istituto di Scienze Marine, Consiglio Nazionale delle Ricerche, Lerici, Italy, and Department of Earth and Planetary Sciences, The Johns Hopkins University, Baltimore, Maryland*

RENSKE GELDERLOOS

*Department of Earth and Planetary Sciences, The Johns Hopkins University, Baltimore, Maryland*

DANA MASTROPOLE

*Woods Hole Oceanographic Institution, Woods Hole, Massachusetts*

(Manuscript received 29 June 2017, in final form 9 October 2017)

## ABSTRACT

Initial results are presented from a yearlong, high-resolution ( $\sim 2$  km) numerical simulation covering the east Greenland shelf and the Iceland and Irminger Seas. The model hydrography and circulation in the vicinity of Denmark Strait show good agreement with available observational datasets. This study focuses on the variability of the Denmark Strait overflow (DSO) by detecting and characterizing boluses and pulses, which are the two dominant mesoscale features in the strait. The authors estimate that the yearly mean southward volume flux of the DSO is about 30% greater in the presence of boluses and pulses. On average, boluses (pulses) are 57.1 (27.5) h long, occur every 3.2 (5.5) days, and are more frequent during the summer (winter). Boluses (pulses) increase (decrease) the overflow cross-sectional area, and temperatures around the overflow interface are colder (warmer) by about  $2.6^{\circ}\text{C}$  ( $1.8^{\circ}\text{C}$ ). The lateral extent of the boluses is much greater than that of the pulses. In both cases the along-strait equatorward flow of dense water is enhanced but more so for pulses. The sea surface height (SSH) rises by 4–10 cm during boluses and by up to 5 cm during pulses. The SSH anomaly contours form a bowl (dome) during boluses (pulses), and the two features cross the strait with a slightly different orientation. The cross streamflow changes direction; boluses (pulses) are associated with veering (backing) of the horizontal current. The model indicates that boluses and pulses play a major role in controlling the variability of the DSO transport into the Irminger Sea.

## 1. Introduction

The Denmark Strait is a deep channel with a  $\sim 620$ -m sill depth located between Iceland and Greenland

(Fig. 1a). It is dynamically relevant to the global climate system because the dense water that overflows through Denmark Strait is a major contributor to the deep western boundary current (DWBC; Dickson and Brown 1994). Indeed, about half of the dense water that feeds the DWBC is supplied by the Denmark Strait overflow (DSO; Dickson et al. 2008; Harden et al. 2016; Jochumsen et al. 2017), making Denmark Strait a critical gateway between the Arctic and subpolar North Atlantic. Several numerical models have been used to

<sup>✉</sup> Supplemental information related to this paper is available at the Journals Online website: <https://doi.org/10.1175/JPO-D-17-0129.s1>.

Corresponding author: Mattia Almansì, [mattia.almansi@jhu.edu](mailto:mattia.almansi@jhu.edu)

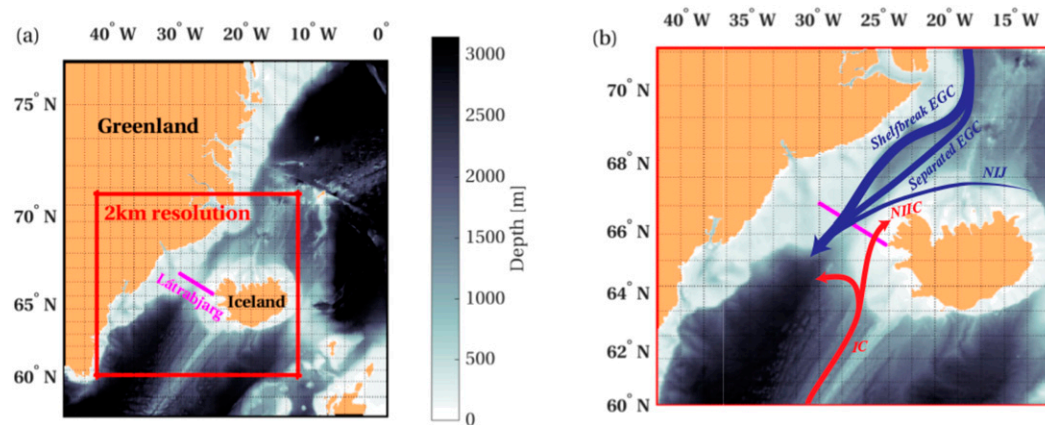


FIG. 1. (a) Plan view of the numerical domain superimposed on seafloor bathymetry. Red lines bound the 2-km resolution area. The Lárabjarg line is drawn in magenta. (b) Schematic of the currents flowing in the 2-km resolution area highlighted in (a). Red (blue) stands for warm (cold) currents. EGC = East Greenland Current, NIJ = North Icelandic Jet, NIIC = North Icelandic Irminger Current, and IC = Irminger Current.

investigate the role of the DSO, and they show its important effects on the Atlantic meridional overturning circulation (AMOC; e.g., Redler and Böning 1997; Schneckendiek and Willebrand 2005; Kösters et al. 2005).

The DSO Water is commonly defined as a mixture of different water masses with a resulting potential density anomaly of more than  $27.8 \text{ kg m}^{-3}$ . In the deepest part of the Denmark Strait trough, the overflow is almost completely composed of dense Arctic-origin water, while less dense Atlantic-origin water and polar surface water contribute to the remainder of the overflow layer (Mastropole et al. 2017). These water masses are advected to the Denmark Strait via three major currents (Fig. 1b): from west to east, (i) the shelfbreak East Greenland Current (EGC; e.g., Strass et al. 1993; Rudels et al. 2002), (ii) the separated EGC (Våge et al. 2013; Harden et al. 2016), and (iii) the north Icelandic jet (NIJ; e.g., Jónsson 1999; Jónsson and Valdimarsson 2004; Våge et al. 2011). A fourth major current crosses Denmark Strait in the opposite direction: it is the North Icelandic Irminger Current (NIIC; Fig. 1b), which is located to the east of the NIJ and brings warm and salty subtropical-origin water into the Iceland Sea (Rudels et al. 2002; Jónsson and Valdimarsson 2012).

Long-term measurements of the DSO transport are available (e.g., Macrandar et al. 2007; Jochumsen et al. 2012, 2015), and the most recent estimate of the average DSO transport is  $3.2 \text{ Sv}$  ( $1 \text{ Sv} = 10^6 \text{ m}^3 \text{ s}^{-1}$ ) with a standard deviation of  $1.5 \text{ Sv}$  (Jochumsen et al. 2017). To understand the overflow transport dynamics, hydraulic control theory has been applied (e.g., Whitehead 1998; Käse and Oschlies 2000; Girton et al. 2001; Helfrich and Pratt 2003; Nikolopoulos et al. 2003; Macrandar et al. 2005; Dickson et al. 2008; Junglaus et al. 2008). Indeed, the volume flux is believed to be modulated by the height of the dense

water above the sill level and the density difference between the upstream and downstream water (Whitehead et al. 1974; Kösters et al. 2005; Köhl et al. 2007).

On a seasonal time scale, there is a discrepancy between the weak observed seasonal variability and the annual cycle simulated by high-resolution models (Biaostoch et al. 2003; Jochumsen et al. 2012). For example, seasonal cycles in the DSO transport time series measured by Jochumsen et al. (2012) and Harden et al. (2014) explain only a small percentage of the variability, while the percentage is about 25% in the model of Köhl et al. (2007). On short time scales, the DSO transport fluctuates markedly (Swaters 1991; Girton et al. 2001) because of mesoscale features with a period of 2–5 days (Ross 1984; Harden et al. 2016). Previous studies have attributed this variability to different processes such as baroclinic instability (Smith 1976) and fluctuations of a weakly depth-dependent jet in the strait (Fristedt et al. 1999).

Using a large number of historical hydrographic sections occupied across the strait, together with 5 years of mooring data, Mastropole et al. (2017) and von Appen et al. (2017) have shed light on two dominant mesoscale features called “boluses” and “pulses.” The term bolus was first introduced by Cooper (1955) and refers to a large lens of cold, weakly stratified overflow water that crosses the strait. The first direct attempt to observe the features motivated by Cooper (1955) was carried out by Harvey (1961). Mastropole et al. (2017) demonstrated that these features are very common and von Appen et al. (2017) found that they are associated with veering of the horizontal current: first toward Iceland, then toward the Irminger Sea, and finally toward Greenland. Numerous other observational and numerical datasets show the existence of these intermittent mesoscale features (e.g.,

Spall and Price 1998; Rudels et al. 1999; Giron and Sanford 2003; Käse et al. 2003; Haine 2010; Magaldi et al. 2011; Koszalka et al. 2013, 2017; Mastropole et al. 2017; von Appen et al. 2017), but the mechanisms that control their formation are still not understood. The term pulse was introduced more recently by Bruce (1995) to describe an intermittent increase in bottom velocity in the strait. Von Appen et al. (2017) demonstrated that these features propagate through the strait approximately every 5 days and are associated with backing: first toward Greenland, then toward the Irminger Sea, and finally toward Iceland. The formation and dynamics of the pulses are also unexplained.

In this study, we advance our understanding of the short-term DSO variability using a high-resolution (horizontal: 2–4 km; vertical: 1–15 m) realistic model centered on Denmark Strait, improving previous configurations available for this area (e.g., Haine et al. 2009; Magaldi et al. 2011; Koszalka et al. 2013; von Appen et al. 2014b; Magaldi and Haine 2015; Gelderloos et al. 2017). Such high resolution allows us to investigate in detail both the boluses and pulses. This has not been possible in past models that are not able to resolve these features. For example, the horizontal resolution used by Logemann et al. (2013) is about 7 km in the Denmark Strait, while the vertical resolution used by Behrens et al. (2017) decreases from 6 m at the surface to 250 m at the bottom. We aim to answer the following questions: 1) How do the overall model hydrography and circulation in Denmark Strait compare with observations from moorings and ship campaigns? 2) Is the observed high-frequency variability of the DSO well captured by the model? 3) How do the hydrography and circulation in Denmark Strait change when boluses and pulses propagate through the region?

The paper is organized as follows: In section 2, we present the high-resolution realistic simulation and describe the methods to identify mesoscale features in the model. We then present our new model dataset in section 3, comparing the model hydrography and circulation in Denmark Strait with previous observational results. We provide significant statistics of the boluses and pulses in section 4, showing the time evolution of these mesoscale features and the spatial distribution of anomalies using composite averages. We summarize our findings and discuss the physical processes that may be involved in section 5.

## 2. Methods

### a. Numerical setup

We have configured a high-resolution realistic numerical model centered on Denmark Strait (Fig. 1a). The dynamics are simulated using the Massachusetts

Institute of Technology General Circulation Model (MITgcm; Marshall et al. 1997). The model solves the hydrostatic Navier–Stokes equations under the Boussinesq approximation for an incompressible fluid, with a nonlinear free surface (Campin et al. 2004). The realistic but simplified equation of state formula by Jackett and McDougall (1995) is implemented, and the K-profile parameterization (KPP; Large et al. 1994) is used.

The model domain has been extended with respect to previous versions (e.g., Haine et al. 2009; Magaldi et al. 2011; Koszalka et al. 2013; von Appen et al. 2014b; Gelderloos et al. 2017) in order to include the entire Iceland Sea to the north as well as Cape Farewell to the southwest (Fig. 1a). The numerical domain is discretized with an unevenly spaced grid of  $960 \times 880$  points; the resolution is 2 km over the center of the domain and decreases moving toward the edges (4-km resolution in the peripheral areas). The vertical domain is discretized by 216 levels, and the vertical grid uses partial bottom cells and the rescaled height coordinate  $z^*$  (Adcroft et al. 2004). The vertical resolution linearly increases from 1 to 15 m in the upper 120 m and is 15 m thereafter. The bathymetry is obtained from the 30-arc-s International Bathymetric Chart of the Arctic Ocean (IBCAO, version 3.0; Jakobsson et al. 2012) north of  $64^\circ\text{N}$  and from Smith and Sandwell (1997) elsewhere and is adjusted using depth data derived from deep-diving seals (Sutherland et al. 2013).

The model was run for 1 year from September 2007 to August 2008 (storing data every 6 h) in order to match the time period of a mooring array deployed across the east Greenland shelf break and slope downstream of Denmark Strait (von Appen et al. 2014a). We performed an 8-month spinup (from January 2008) initialized with the global  $1/12^\circ$  reanalysis HYCOM + NCODA (Cummings and Smedstad 2013) and the monthly reanalysis Toward an Operational Prediction System for the North Atlantic European Coastal Zones, version 4 (TOPAZv4; Sakov et al. 2012). HYCOM + NCODA is also used to nudge the velocities, temperature, and salinity at the four open boundaries. Sea surface temperature is relaxed to the Operational Sea Surface Temperature and Sea Ice Analysis (OSTIA) global product (Donlon et al. 2012), while surface forcings (air temperature, specific humidity, wind, evaporation, precipitation, and radiation) are based on the global atmospheric reanalysis ERA-Interim (Dee et al. 2011).

The oceanic component is coupled with the MITgcm sea ice model (Losch et al. 2010). TOPAZv4 is used to nudge sea ice area, thickness, salinity, and snow and ice velocities at the boundaries; the nudging time scale is 1 day at each boundary and linearly increases toward the

interior to reach a maximum value of 10 days at 20 grid points from the boundary. The freshwater forcing is improved with respect to previous configurations: (i) surface runoff is estimated from a dataset of daily, 1-km resolution Greenland Ice Sheet surface mass balance (Noël et al. 2016), and (ii) solid ice discharge is estimated from a combination of climate modeling plus satellite and terrestrial data (Bamber et al. 2012) and is distributed over the oceanic grid cells adjacent to Greenland [a similar approach has been used by Bakker et al. (2012)].

### b. Identification of mesoscale features

As discussed above, boluses and pulses are dominant mesoscale features of the overflow water in Denmark Strait. Mastropole et al. (2017) recently characterized the structure and properties of boluses using a large collection of hydrographic sections occupied across the strait, while von Appen et al. (2017) compared the hydrographic and kinematic structure of boluses and pulses, augmenting the dataset used by Mastropole et al. (2017) with mooring data. Von Appen et al. (2017) deduced that both boluses and pulses increase the southward DSO transport. In the former case this is dictated primarily by the increase in cross-sectional area of the water denser than  $27.8 \text{ kg m}^{-3}$ , while in the latter case it is due mainly to an enhancement of the near-bottom flow. It should be noted, however, that von Appen et al. (2017) had data from only one mooring located in the center of the strait.

Here, we have developed an objective method to identify boluses and pulses in our model vertical sections. Specifically, a set of thresholds was applied in the region from 15 km west to 15 km east of the deepest part of the sill (black dashed lines in Fig. 2). In step 1, a vertical section was identified as containing a potential mesoscale feature if the southward overflow transport was greater than the yearly 25th percentile (considering the equatorward transport positive). In step 2, if the overflow cross-sectional area was smaller (larger) than the yearly 35th (65th) percentile, then the vertical section was deemed to contain a pulse (bolus). If the overflow transport or cross-sectional area thresholds were not exceeded, the vertical section was considered to be representative of the background state. Thus, cases where there is a large DSO transport but the overflow interface does not deepen or shoal were considered as background state. Moreover, the few cases where the cross-sectional area of the overflow changes with a low DSO transport were considered background state as well. To be consistent with the observed overflow transport, cross-sectional area, and repeated occurrences of boluses and pulses, we calibrated our

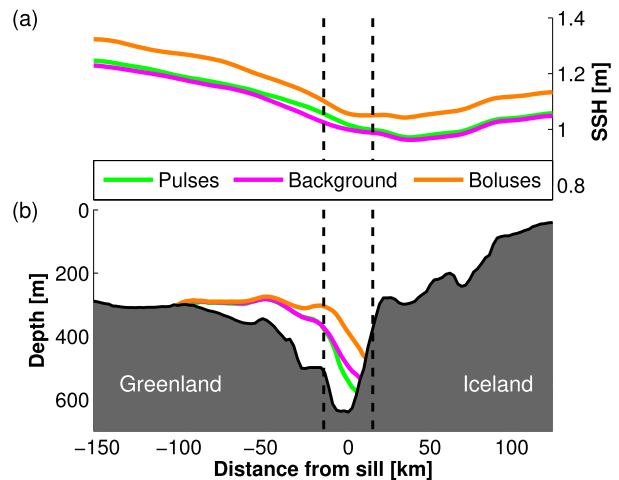


FIG. 2. Composites of (a) SSH and (b) DSO interface during boluses (orange), pulses (green), and background state (magenta). Black dashed lines bound the region from 15 km west to 15 km east of the deepest part of the sill. Negative (positive) distances correspond to northwest (southeast) of the sill. The viewer is looking to the north.

thresholds (percentiles) using the statistics determined by von Appen et al. (2017; see section 4a).

The mean cross-strait structures of the interface height for the two types of model mesoscale features are consistent with the observations. Figure 2b reveals that the maximum displacement of the DSO interface occurs in the middle of the strait for both types of features. Furthermore, the sea surface height (SSH) across Denmark Strait rises everywhere by 4–10 cm during the passage of boluses and by up to 5 cm in the western side of the strait during pulses (Fig. 2a). Thus, our composites of boluses and pulses suggest that altimeter data may be used to detect these mesoscale features. This is consistent with the correspondence between fluctuations in the time series of the Denmark Strait transport (DST) and SSH anomalies found by Haine (2010). SSH data have been used to estimate the DST (e.g., Lea et al. 2006), and Haine (2010) argued that the DST may be inferred from SSH data using a retrospective analysis, models, and data assimilation. See the supplemental information for an animation of SSH (cyan) and height of the DSO interface during boluses (orange), pulses (green), and background state (magenta).

One of the features of the overflow boluses described by Mastropole et al. (2017) is their weak stratification. Their method to identify boluses was also based on a Brunt–Väisälä frequency ( $N^2$ ) criterion. Although our method does not employ any stratification thresholds, the overflow  $N^2$  in the model during bolus events is consistent with the definition provided by Mastropole et al. (2017). Indeed, the comparison between the model



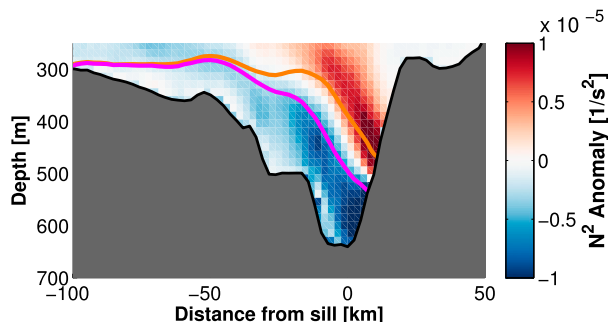


FIG. 3. Composite of boluses minus background state Brunt-Väisälä frequency. The orange (magenta) line corresponds to the composite of boluses (background state) DSO interface.

composites of boluses and the background state shows that the overflow layer is more weakly stratified during the passage of boluses, especially on the eastern side of the trough where  $N^2$  is lower by about  $10^{-5} \text{ s}^{-2}$  (Fig. 3).

### 3. Comparison with observations

#### a. Hydrography

We now compare the model output in Denmark Strait with conductivity-temperature-depth (CTD) data from the 111 shipboard transects occupied between March 1990 and August 2012 analyzed by Mastropole et al. (2017). Most of the sections were done by the Marine and Freshwater Institute of Reykjavik as part of their quarterly surveys; hence, there is good coverage throughout the different seasons (see <http://www.hafro.is/Sjora/>). In their study, Mastropole et al. (2017) projected the stations onto the Látrabjarg standard section ( $66.9^\circ\text{N}$ ,  $29.8^\circ\text{W}$ ;  $65.5^\circ\text{N}$ ,  $24.6^\circ\text{W}$ ; Fig. 1a) and interpolated each section in depth space in the upper layer and in density space in the lower. Their mean hydrographic sections are reproduced in Figs. 4a, 4c, and 4e. We performed the same procedure on the model outputs. Specifically, the model fields were evaluated at the grid points corresponding to the location of the observational stations; then vertical sections were constructed by projecting and interpolating the numerical data using the hybrid interpolator. We note that the observational data were sampled over a  $\sim 20$ -yr period, while the model was run for only 1 year. To match the seasonal distribution of the observations, the model was subsampled at the same relative yearday corresponding to the stations. The mean model hydrographic sections are shown in Figs. 4b, 4d, and 4f.

Overall, the agreement between the model and the observations is excellent. The model captures all of the major water mass features in Denmark Strait, including the warm, salty subtropical-origin (Irminger) water on

the Iceland shelf; the cold, fresh Arctic-origin water extending from the western boundary into the strait; the relatively warm recirculated Irminger Water on the Greenland shelf; and the cold, dense overflow water in the trough. In addition, the model isopycnal structure across the strait is very similar to that seen in the observations. We also compare the spatial distribution of model Brunt-Väisälä frequency (Fig. 4f) with observations (Fig. 4e). In both cases the overflow water is weakly stratified, as is the deep portion of the Irminger Water on the Iceland shelf. Quantitatively, however, there are some differences between the model fields and the observations. The Arctic-origin water on the east Greenland shelf in the model is too cold and fresh, while the model overflow water is too warm by about  $1^\circ\text{C}$  in the deepest part of the trough. Because of this, the measured overflow interface ( $27.8 \text{ kg m}^{-3}$  isopycnal) corresponds approximately to the  $27.7 \text{ kg m}^{-3}$  isopycnal in the model (contours in Fig. 4). These biases can be due to interannual variability and model errors. However, since Macrande et al. (2005) and Jochumsen et al. (2012) found warm events in the 2000s (measured overflow temperatures were warmer by about  $0.5^\circ\text{C}$  than the average temperature), interannual variability may be the predominant factor.

Mastropole et al. (2017) described two fronts in their mean hydrographic sections (Figs. 4a,c) that cannot be reproduced by lower-resolution models (e.g., Logemann et al. 2013; Filyushkin et al. 2013; Behrens et al. 2017). One front is located in the center of the strait, which, according to the authors, corresponds to the separated EGC. The second front is located near the Greenland shelf break and corresponds to the shelfbreak EGC. Both of these fronts exist in our model and are located in roughly the same area as the observations. This is particularly evident in the model temperature section, which shows that the coldest water in the upper layer is west of the east Greenland shelf break, while the warmest water is confined to the Iceland shelf. As was the case with the observations, these frontal features are sometimes difficult to detect in individual model sections, which demonstrates the value of constructing means.

The uneven sampling in time and space was performed on the model output with the goal of making an optimal comparison with the observations. Hereafter, we estimate the Denmark Strait properties by fully sampling the model at the grid points along the Látrabjarg line. Estimating the mean annual properties with 6-h regular sampling we found that mean sections obtained using the uneven sampling are consistent. This was especially true on the Iceland shelf where the majority of the measurements were taken (Fig. 5a). With a mean absolute anomaly of

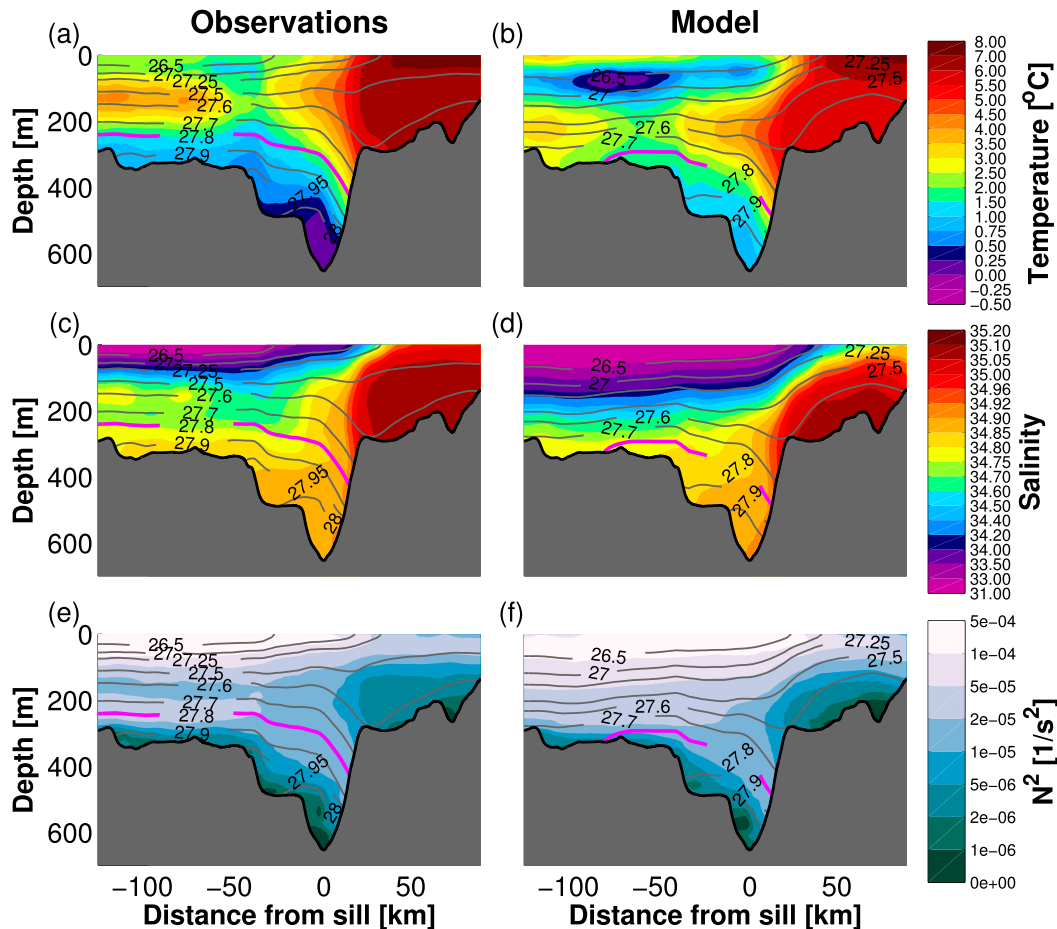


FIG. 4. Time-mean vertical sections obtained from (left) observations (Mastropole et al. 2017) and (right) model outputs: (a),(b) potential temperature, (c),(d) salinity, (e),(f) Brunt-Väisälä frequency and potential density anomaly ( $\text{kg m}^{-3}$ ; contours). The DSO interface is highlighted in magenta.

approximately  $1^{\circ}\text{C}$ , temperature is the most biased field (Fig. 5b). Regularly sampled temperatures are colder on the Greenland shelf by about  $2^{\circ}\text{C}$ , and the eastern flank of the trough is slightly warmer. By contrast, biases in salinity and density are generally small and very localized (Figs. 5c,d); the regular sampling produces slightly fresher and lighter water in the westernmost area of the strait, while denser and saltier water is found in the upper 100 m in the center of the strait. Biases on the western side of Denmark Strait are mainly due to the dearth of measurements, while biases in the center of the strait are mainly due to the uneven time distribution of the observations. For example, fall is the season with the largest number of samples (about 33% of the transects). Figure 5d shows that the uneven sampling in Mastropole et al. (2017) produces densities in the deepest part of the trough and below  $\sim 200$  m on the Greenland shelf that are consistent with the regular sampling. Thus, the

isopycnal contours in Fig. 4 accurately represent the yearly mean densities in the strait.

#### b. Circulation

Using data from a shipboard survey in October 2008, Våge et al. (2011) computed the absolute geostrophic velocity normal to the Látrabjarg section (Fig. 6a). This synoptic realization shows that the DSO Water flowing southward is banked against the Greenland side of the trough, while the subtropical-origin water flows northward on the eastern side of the trough in the NIIC (Rudels et al. 2002). These two currents are well captured in the mean October 2007 model velocity section (Fig. 6b). The mean model section also shows lighter DSO flowing equatorward near the Greenland shelf break, which is consistent with the results of Mastropole et al. (2017), who demonstrate that Atlantic-origin DSO is found in this region. While the 2008 synoptic section of Våge et al. (2011) contains more complex flow structure

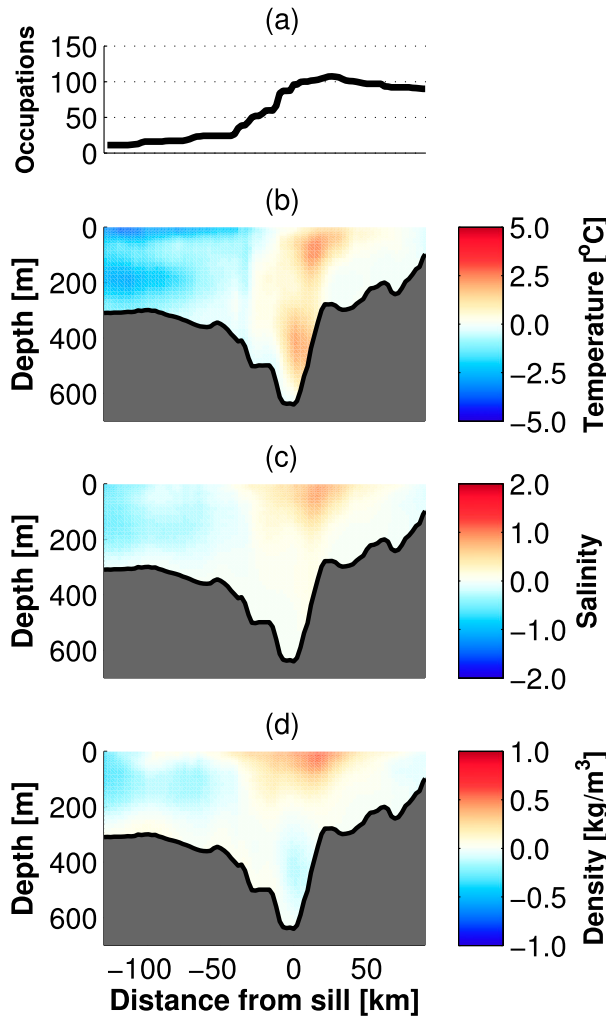


FIG. 5. (a) Data coverage of the vertical sections. Anomalies of (b) potential temperature, (c) salinity, and (d) potential density for the regular minus the uneven sampling.

than the mean model section, this is due to the energetic short time scale variability of the dynamics in the Denmark Strait. Indeed, model snapshots display similar mesoscale variability, such as the 1 October 2007 realization (Fig. 6c). Unlike the hydrographic fields, we are unable to address velocity biases in the model since there are no mean velocity sections based on observations. Nonetheless, the model data similarities in Fig. 6 are encouraging.

#### 4. Results

##### a. Statistics of boluses and pulses

On average, boluses occur in the model every 3.2 days, while pulses pass through the Denmark Strait every 5.5 days. This is remarkably similar to the observations of von Appen et al. (2017; 3.4 and 5.4 days, respectively,

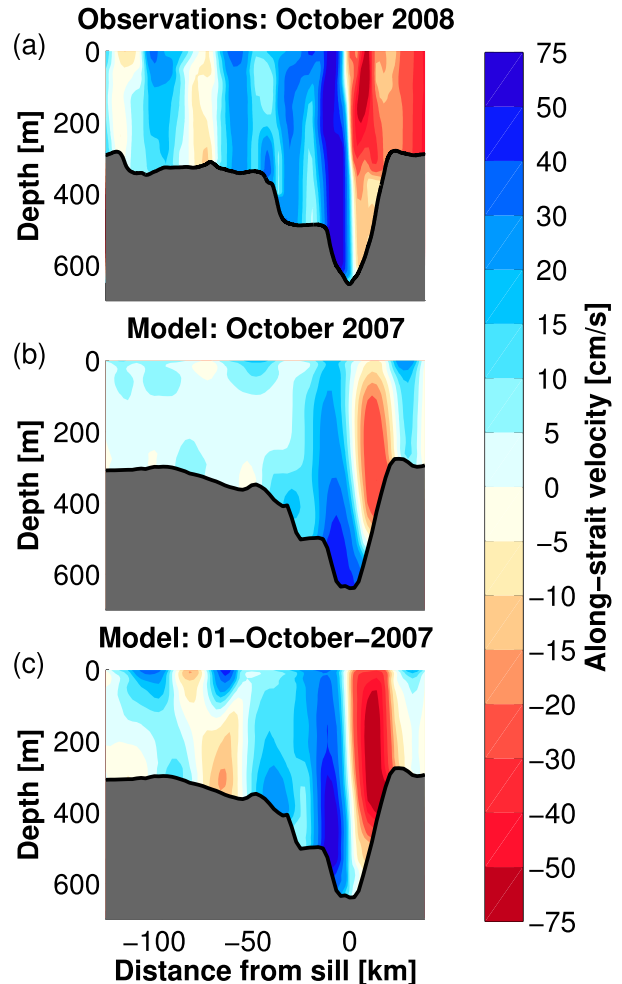


FIG. 6. Vertical sections of (a) absolute geostrophic velocity measured in October 2008 (Våge et al. 2011), (b) monthly mean model velocity of October 2007, and (c) mean model velocity on 1 Oct 2007. The direction of the velocity fields is normal to the Láttrabjarg line (equatorward flow is positive).

for boluses and pulses). Thus, 31% (18%) of the vertical sections have been labeled as boluses (pulses), while about half of them do not contain any pronounced mesoscale feature. As was true in the observations (von Appen et al. 2017), pulses are associated with stronger southward velocities than boluses. Averaging over the area 15 km west to 15 km east of the deepest part of the sill (black dashed lines in Fig. 2), the mean along-strait equatorward speed of a pulse is  $0.43 \text{ m s}^{-1}$  versus  $0.27 \text{ m s}^{-1}$  for a bolus (background state is  $0.24 \text{ m s}^{-1}$ ), while the mean cross-strait westward speed of a pulse is  $0.29 \text{ m s}^{-1}$  for a bolus (background state is  $0.14 \text{ m s}^{-1}$ ). The model reveals that the direction of the DSO is skewed relative to the along-strait direction (Fig. 7). Furthermore, Fig. 7 shows that the direction of boluses (pulses) is slightly tilted toward Iceland (Greenland).

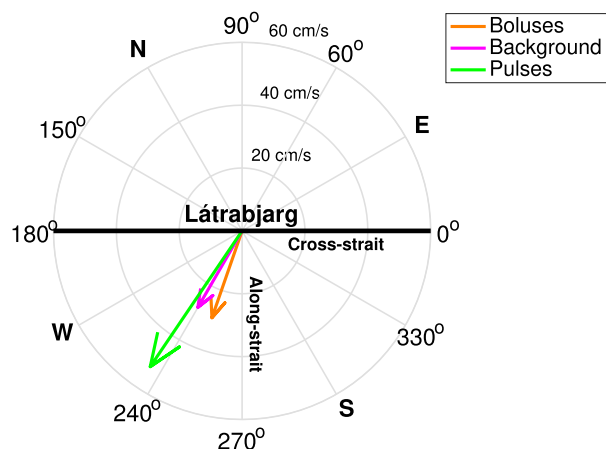


FIG. 7. Mean velocity of the DSO between 15 km west and 15 km east of the sill in the composites of boluses (orange), pulses (green), and background state (magenta). The thick black line corresponds to the direction of the Látrabjarg line (cross strait).

The mean southward DSO volume flux (transport) excluding boluses and pulses is by definition smaller than the mean transport estimated using all of the vertical sections. However, the model allows us to quantify the contribution of boluses and pulses to the yearly mean DSO volume flux, and we estimate that, excluding the mesoscale features, the transport is lower by about 30%.

In contrast with Mastropole et al. (2017) and von Appen et al. (2017), who did not find any seasonal signal, the model suggests that between September 2007 and August 2008 boluses and pulses are not evenly distributed throughout the year (Fig. 8). Model boluses are more frequent during summer 2008, and pulses occur more frequently in winter 2007–2008. Roughly 40% of boluses cross Denmark Strait between June and August 2008, while the frequency is lower in fall 2007 and spring 2008, and the minimum occurs between December 2007 and February 2008. Conversely, more than 30% of pulses occur in winter 2007–08, and only 17% cross the strait in summer 2008. While these trends offset each other to some extent, the model suggests that the majority of the energetic mesoscale features occur in summer 2008 (~30%).

#### b. Time evolution of mesoscale features

On average, bolus events are  $57.1 \pm 48.7$  h long ( $\pm$  indicates standard deviations) and pulses are  $27.5 \pm 15.4$  h long, although both types of events can last from anywhere between a few hours to a few days. We now construct a composite of each type of event to shed light on their temporal evolution. We average together all of the boluses whose duration is between 47.1 and 67.1 h, which results in 13 events. Some of the pulses are asymmetric in their along-strait structure, so these are excluded from the

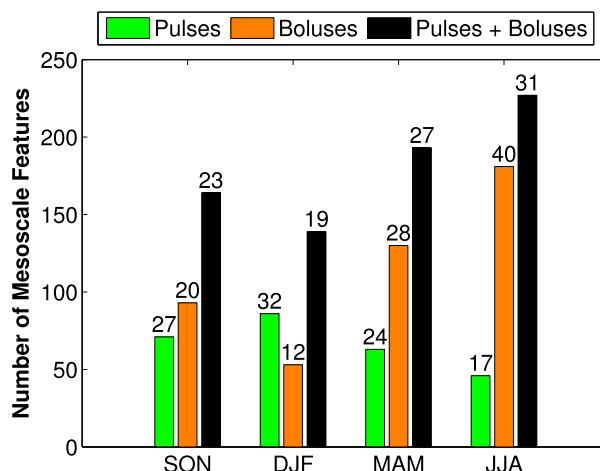


FIG. 8. Seasonality of boluses and pulses. Green (orange) bars show the number of pulses (boluses) in a season. Black bars show the seasonal distribution of boluses + pulses. The numbers on the top of the bars indicate the percentage of boluses, pulses, or boluses + pulses in a season compared to the total number of boluses, pulses, or boluses + pulses, respectively. The 3-month acronyms for seasons are SON, DJF, MAM, and JJA.

pulse composite, and 12 events are considered. Our rationale is to focus on the canonical features and to have similar numbers of realizations in each average. The time-depth composites for hydrography are shown in Fig. 9 and for velocity are shown in Fig. 10. These are obtained by averaging spatially over the area between 15 km west and 15 km east of the deepest part of the sill (black dashed lines in Fig. 2). We normalized each bolus and pulse before creating composites, and we use a normalized time axis corresponding to the length of the events.

As expected, boluses correspond to an enhanced presence of cold, weakly stratified overflow water and a shallowing of the  $27.8 \text{ kg m}^{-3}$  interface (Figs. 9a,c). By contrast, pulses are characterized by a thinning of the overflow layer and depression of the interface (Figs. 9b,d). There are clear differences in the middle of the water column as well between the two features; boluses contain slightly colder and fresher water, while there is a large presence of warm and salty Irminger Water at middepth during a pulse. Both of these signals are consistent with the findings of von Appen et al. (2017). For the latter case, von Appen et al. (2017) showed that the passage of a pulse coincides with a westward shift in the hydrographic front associated with the Irminger Water over the Iceland shelf.

For the time-depth velocity composites we show the along-stream and cross-stream velocities (instead of the along-strait and cross-strait components). The reason is that boluses and pulses cross the strait with slightly different directions (Fig. 7). As the mean velocity vectors in the overflow layer of the composites in Fig. 10 agree with the mean velocity vectors computed considering every



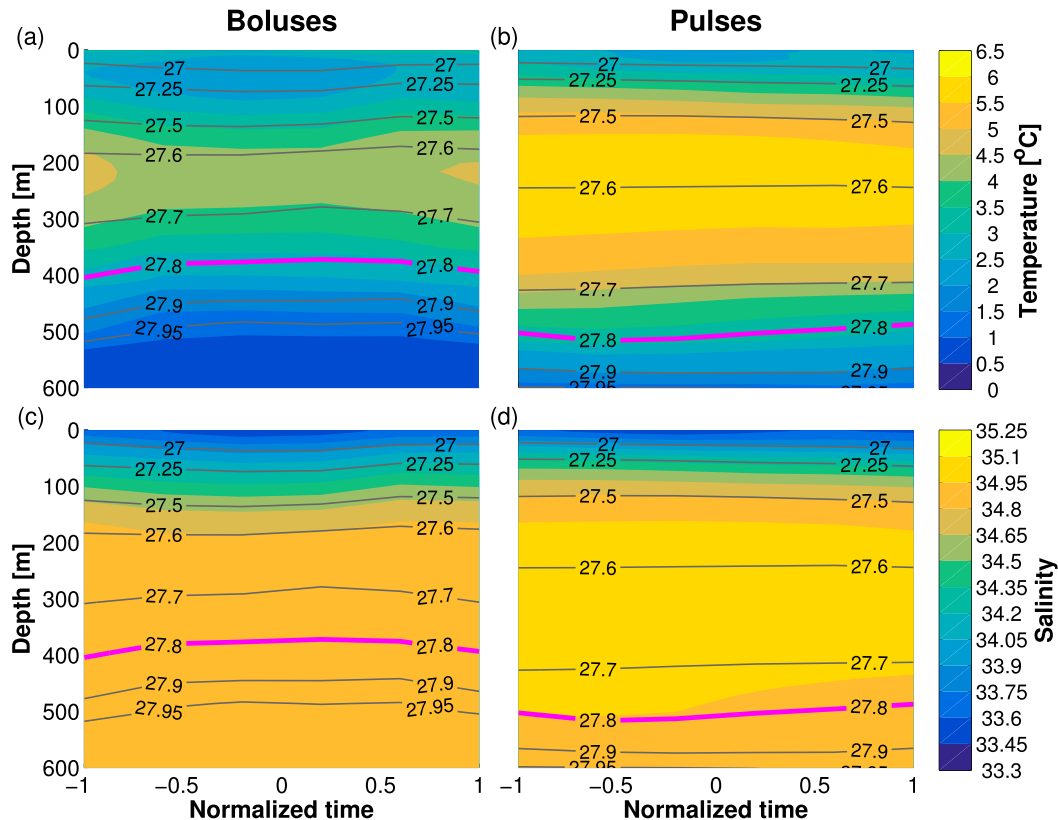


FIG. 9. Time evolution of the composites of representative (left) boluses and (right) pulses obtained by averaging (a),(b) potential temperature and (c),(d) salinity over the area between 15 km west and 15 km east of the sill. The time axis is normalized to the length of the events ( $57.1 \pm 10$  h for boluses and  $27.5 \pm 15.4$  h for pulses). The potential density contours are drawn in gray and the DSO interface is highlighted in magenta.

bolus and pulse, the along-stream direction for boluses and pulses is defined as the orientation of the mean velocity vectors in Fig. 7. This revealed a kinematic structure that is very much in line with the observations. For boluses, there is no consistent variation in the along streamflow of DSO Water. However, there is a very clear pattern in the cross-stream velocity for the upper layer that extends into the overflow layer as well. Specifically, the flow is toward Iceland at the leading edge of the bolus and toward Greenland at the trailing edge, indicating that boluses are associated with veering. For pulses, the along streamflow of DSO Water is significantly faster in the center of the feature, while the cross streamflow is associated with backing: first toward Greenland and then toward Iceland. All of these characteristics agree with the observational composites presented by von Appen et al. (2017; although the DSO cross-stream velocities are slightly larger in the model).

### c. Spatial distribution of anomalies

We also use composites to examine the spatial distribution—both in the vertical plane and horizontal plane—of

boluses and pulses as they progress through the strait. These composites include every snapshot identified as bolus, pulse, or background. Thus, the averages in Figs. 11 and 12 represent the mesoscale features when they are centered at the Látrabjarg line.

As shown in Figs. 9c and 9d, the intermediate water is slightly saltier during pulses and fresher during boluses ( $\Delta S \leq 0.05$ ), while anomalies in the overflow layer are negligible. These small salinity anomalies of the intermediate water are uniformly distributed across Denmark Strait, so salinity is omitted in Fig. 11. However, there is a clear temperature anomaly in the vertical plane associated with each feature. The temperature in the trough is up to  $2.6^\circ\text{C}$  colder during bolus events with the cold water mainly concentrated around the overflow interface (Fig. 11a), although the anomaly extends more than 200 m above the  $27.8 \text{ kg m}^{-3}$  isopycnal. The largest temperature difference occurs on the eastern flank of the trough. By contrast, the temperature at the overflow interface increases by up to  $1.8^\circ\text{C}$  during pulses (Fig. 11b). The largest difference again occurs on the eastern flank (same as boluses), but it is smaller.

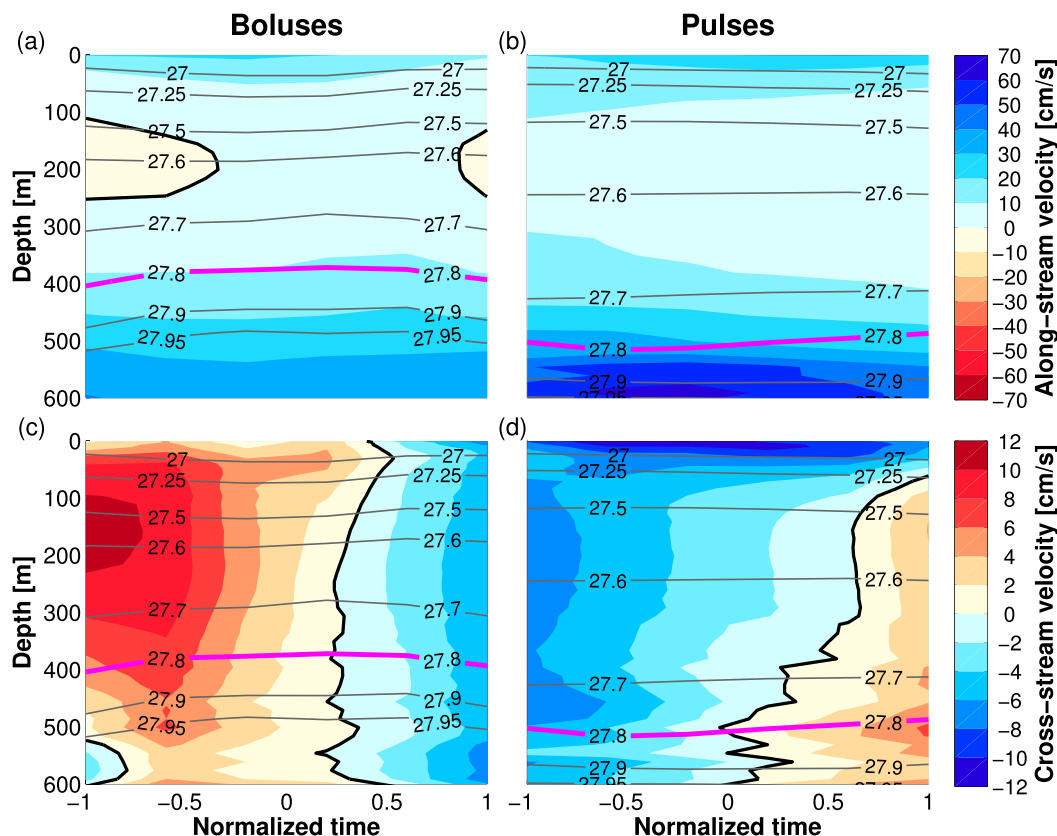


FIG. 10. As in Fig. 9, but for (a),(b) along-stream velocity, and (c),(d) cross-stream velocity. The along-stream direction for boluses and pulses is defined as the orientation of the mean velocity vectors in Fig. 7. Zero velocity contours are drawn in black.

Interestingly, there is no surface temperature signal within the trough during the passage of boluses and pulses (Figs. 11a,b). Indeed, the time series in the region where our thresholds are applied do not show any clear link between surface temperature variability and mesoscale features (Figs. 9a,b). Surface temperature anomalies are only present in the composite of boluses and are located on the Iceland shelf, where the surface water is warmer by up to  $1.4^{\circ}\text{C}$ . There are also well-defined anomalies in the vertical plane for the along-strait velocity. While the flow of DSO Water is enhanced in each case, the composites reveal that there are differences in structure. During pulses, the signature is confined to the overflow layer (Fig. 11d). The DSO increases by more than  $30\text{ cm s}^{-1}$ , and the maximum anomaly occurs on the western flank of the trough. This large increase in speed is associated with the enhancement of the overflow transport together with the compression of the overflow layer. By comparison, the along-strait velocity anomaly of the boluses is smaller ( $<25\text{ cm s}^{-1}$ ; Fig. 11c), although the entire water column is impacted and there is anomalous northward flow as

well. The enhanced southward flow is located in the center of the strait, while the northward anomaly is near the Iceland shelf break. This suggests that there is a link between the boluses and the poleward flow of the NIIC.

Finally, we constructed lateral composites of the DSO interface height and SSH, and differenced these from the background state to create anomalies (Fig. 12). Consistent with the vertical plane perspective shown above, the interface deflection at the sill is much more pronounced for boluses than pulses. On average, the DSO interface shoals by up to 85 m during boluses and deepens by up to 50 m during pulses. Thus, boluses occupy a larger cross-sectional area than pulses. Both boluses and pulses have an elongated shape: the along-strait horizontal length scale is larger than the cross-strait horizontal length scale. Notably, the lateral scales of the two features are quite different, and boluses also occupy a larger horizontal area. Furthermore, during the passage of a bolus the interface height is elevated throughout the Denmark Strait. This is markedly different than pulses where the interface is depressed over a relatively confined region, surrounded by a modest

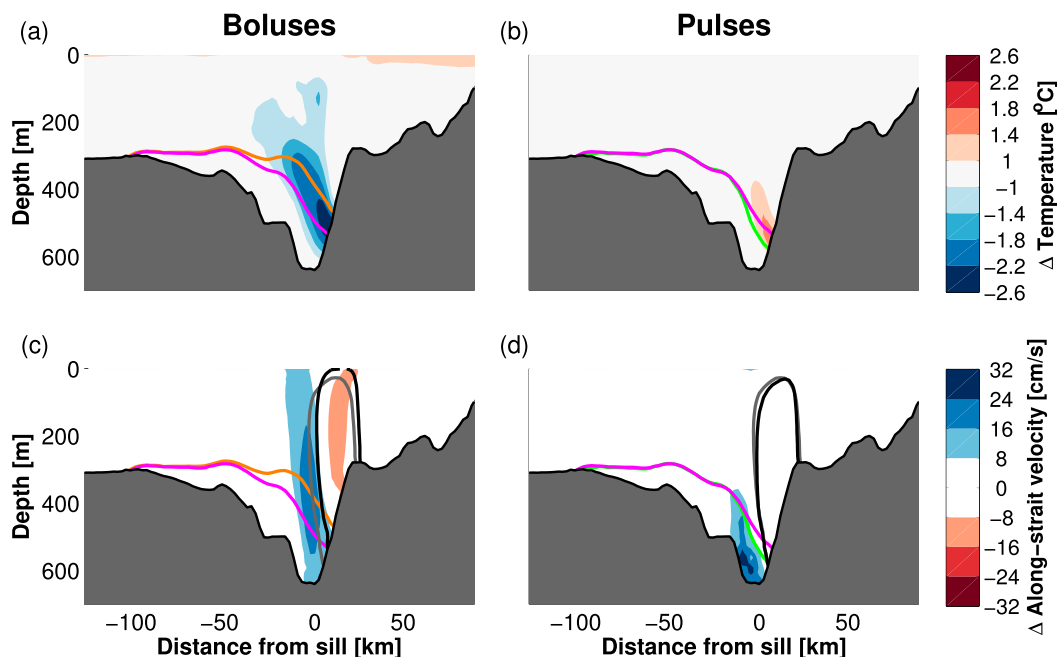


FIG. 11. Composites of (left) boluses and (right) pulses minus the background state: (a),(b) potential temperature and (c),(d) along-strait velocity. Positive velocities are equatorward. The DSO interface during boluses (orange), pulses (green), and background state (magenta) are outlined. Gray contours bound the northward flow at the Iceland shelf break during the background state, while black contours bound the northward flow during boluses in (c) and pulses in (d).

increase in layer height. SSH anomaly contours reveal a relative minimum upstream of the sill for a bolus and a relative maximum upstream of the sill for a pulse (black contours in Fig. 12). These surface anomalies are offset in the along-strait direction with the DSO interface anomalies. Composites of the vertical component of the relative vorticity [ $\zeta = (\partial v / \partial x) - (\partial u / \partial y)$ ] do not show any clear pattern associated with boluses or pulses. Thus, the mean shallow-water potential vorticity (PV) of the overflow water [ $PV = (\zeta + f)/h$ ] is highly influenced by the height of the overflow interface, and PV anomaly maps look similar to Fig. 12; the mean PV of the overflow layer increases during pulses and decreases during boluses.

## 5. Summary and discussion

We have presented first results from a yearlong run of a high-resolution realistic numerical model centered on Denmark Strait. This dataset and user-friendly postprocessing tools are publicly available on SciServer (<http://www.sciserver.org/integration/oceanography/>; Medvedev et al. 2016), and we provide a Jupyter Notebook to reproduce the figures in this paper that only involve the model output (<https://doi.org/10.7281/T1Q52MS4>). It was demonstrated that the model hydrographic and velocity fields in the vicinity of the strait are consistent with available observational datasets. Even though the model outputs are slightly warmer in

the trough, the temperature biases only affect the density in the deep part of the water column (the magnitude of density biases is about  $0.1 \text{ kg m}^{-3}$ ). However, the choice of the density that defines the overflow interface does not affect the results of this study (overflow transport and cross-sectional area thresholds are based on percentiles).

Our study focused on the variability of the hydrography and circulation in Denmark Strait caused by the passage of boluses and pulses. These have been previously identified in observations as the two dominant mesoscale features in the strait, both of which increase the overflow transport. To detect the boluses and pulses, we used an objective method based on transport and cross-sectional area of the DSO using the statistics provided by von Appen et al. (2017) to calibrate our thresholds.

The general properties of the two types of features are summarized in Table 1. Boluses occur more frequently than pulses and are of longer duration. The DSO interface shoals during boluses and deepens during pulses, and the along-strait length scale of the boluses is larger. SSH rises during the passage of both mesoscale features. SSH anomaly contours form a bowl upstream of Denmark Strait during boluses, while during pulses they form a dome centered northwest of the sill. Seasonally, boluses are more common in summer 2008, while pulses appear more often in winter 2007–08.

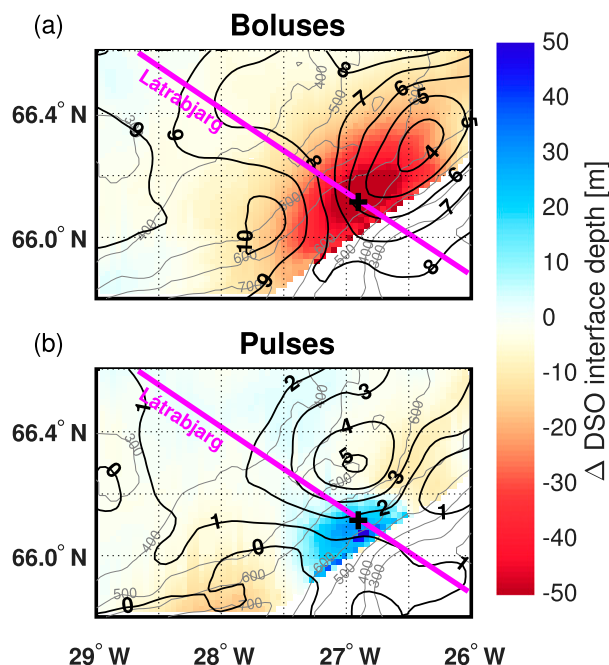


FIG. 12. Composite of DSO interface during (a) boluses and (b) pulses minus the background state. Black contour lines show the SSH composite during boluses and pulses minus the background state (cm). The bathymetric contours (m) are shown in gray. The Láttrabjarg line is drawn in magenta, and the black cross corresponds to the sill. Regions where the entire water column is lighter than the overflow water are masked white. Negative (positive) anomalies correspond to a shallower (deeper) DSO compared to the background state.

By constructing composite averages of the two types of features we quantified their temporal and spatial structure. Boluses correspond to a thicker, colder, more weakly stratified layer of DSO with moderately enhanced equatorward velocity. Above the overflow water, the Atlantic layer becomes slightly colder and fresher and there is a strong cross-stream velocity signature indicative of veering. By contrast, pulses are characterized by a thinning of the DSO layer and a stronger increase in equatorward velocity. Warm and salty Irminger Water appears in the middle of the water column, and the cross streamflow is again strong above the overflow layer—except in this case it is indicative of backing. These features are in line with the observations of Mastropole et al. (2017) and von Appen et al. (2017).

The high-resolution, three-dimensional model fields allow us to go beyond the observations. We determined that the temperature anomalies are strongest near the overflow interface; in particular, water near the interface of the overflow layer is colder by about  $2.6^{\circ}\text{C}$  during boluses and warmer by about  $1.8^{\circ}\text{C}$  during pulses. The enhanced equatorward flow during pulses is confined to

TABLE 1. Summary of boluses and pulses mean properties and thresholds.

Thresholds and properties	Boluses	Pulses
DSO transport threshold (percentile)	>25	>25
Cross-sectional area threshold (percentile)	>65	<35
Mean duration (h)	57.1	27.5
Frequency of occurrence (days)	3.2	5.5
Mean along-strait velocity ( $\text{m s}^{-1}$ )	0.27	0.43
Mean cross-strait velocity ( $\text{m s}^{-1}$ )	0.09	0.29
Maximum $\Delta\text{DSO}$ interface depth <sup>a</sup> (m)	−85	+50
$\Delta\text{SSH}$ (cm)	4–10	0–5
$\Delta T$ at the DSO interface ( $^{\circ}\text{C}$ )	−2.6	+1.8
$\Delta S$ of the DSO	$\approx 0$	$\approx 0$
Rotation of the DSO direction over time	Veering	Backing

<sup>a</sup> Negative anomaly corresponds to shallower DSO interface relative to the background state.

the overflow layer on the western side of the trough, while for boluses it extends throughout the water column in the center of the trough. Interestingly, the poleward flow of the NIIC increases during bolus events. The lateral extent of the boluses is much greater than that of the pulses, and the DSO interface is raised throughout Denmark Strait. By contrast, the interface is depressed over a much smaller region during pulses, and in the surrounding area it is slightly raised. We find that the mean southward transport of the DSO is about 30% lower in the absence of boluses and pulses. Thus, these features play a major role in controlling the variability of the DSO transport. Combining our high-resolution model with longer model runs (e.g., Behrens et al. 2017) and observational datasets of the DWBC (e.g., Fischer et al. 2015) will enable a better understanding of the impacts of the high-frequency DSO variability on the AMOC.

Although a complete understanding of the dynamics that control these energetic mesoscale features is beyond the scope of this paper, we provide a brief description of the physical processes that may be involved. We found that boluses and pulses have a clear signature in SSH anomaly; boluses are associated with a relative minimum upstream of the sill, while pulses are associated with a relative maximum upstream of the sill. Assuming that the flow is geostrophic, these anomalies imply enhanced DSO flow toward Iceland during boluses (cyclonic) and toward Greenland during pulses (anticyclonic), consistent with the flow vectors shown in Fig. 7. Similar to the western tilt with height that occurs in the midlatitude weather systems, the SSH and DSO interface anomalies are not in phase. Idealized models of baroclinic instabilities (e.g., Eady 1949) show how this lag implies the release of available potential energy and conversion to eddy

kinetic energy (e.g., Pedlosky 1979; Vallis 2006). While Fischer et al. (2015) found that topographic waves with periods of 10 days dominate the variability of the DWBC downstream of Denmark Strait in the Irminger and Labrador Seas, the dynamics controlling the shorter-period variability at the sill remain unclear. Mooring data analyzed by Jochumsen et al. (2017) suggest that fluctuations in DSO transport form upstream of Denmark Strait. Thus, coastally trapped waves triggered by upstream downwelling-favorable winds (Harden et al. 2014) could play a role in controlling the pulsating behavior of the DSO transport.

At this point it is also uncertain if the boluses and pulses are associated with different dynamical processes. The formation of pulses and the corresponding wavelike deformation of the DSO interface (alternating positive/negative DSO interface anomalies) may be explained by the baroclinic destabilization of density-driven abyssal flows theorized by Reszka et al. (2002). On the other hand, boluses are associated with an enhanced equatorward flow throughout the whole water column and may be related to the NIJ (Mastropole et al. 2017). Further work using this model and different configurations (e.g., applying a different atmospheric forcing) will address the mechanisms that control the NIJ variability and the evolution of boluses, allowing us to establish a cause-and-effect relationship between boluses and the Denmark Strait variability described in this paper.

**Acknowledgments.** This work was supported by the NSF Grants OCE-1433448, OCE-1633124, and OCE-1259618 and the Institute for Data Intensive Engineering and Science (IDIES) seed grant funding. The numerical model was run on the Maryland Advanced Research Computing Center (MARCC) and the postprocessing was performed on the Johns Hopkins Data-Scope.

## REFERENCES

- Adcroft, A., J.-M. Campin, C. Hill, and J. Marshall, 2004: Implementation of an atmosphere–ocean general circulation model on the expanded spherical cube. *Mon. Wea. Rev.*, **132**, 2845–2863, <https://doi.org/10.1175/MWR2823.1>.
- Bakker, P., C. J. Van Meerbeeck, and H. Renssen, 2012: Sensitivity of the North Atlantic climate to Greenland Ice Sheet melting during the last interglacial. *Climate Past*, **8**, 995–1009, <https://doi.org/10.5194/cp-8-995-2012>.
- Bamber, J., M. van den Broeke, J. Ettema, J. Lenaerts, and E. Rignot, 2012: Recent large increases in freshwater fluxes from Greenland into the North Atlantic. *Geophys. Res. Lett.*, **39**, L19501, <https://doi.org/10.1029/2012GL052552>.
- Behrens, E., K. Våge, B. Harden, A. Biastoch, and C. W. Böning, 2017: Composition and variability of the Denmark Strait Overflow Water in a high-resolution numerical model hindcast simulation. *J. Geophys. Res. Oceans*, **122**, 2830–2846, <https://doi.org/10.1002/2016JC012158>.
- Biastoch, A., R. H. Käse, and D. B. Stammer, 2003: The sensitivity of the Greenland–Scotland Ridge overflow to forcing changes. *J. Phys. Oceanogr.*, **33**, 2307–2319, [https://doi.org/10.1175/1520-0485\(2003\)033<2307:TSOTGR>2.0.CO;2](https://doi.org/10.1175/1520-0485(2003)033<2307:TSOTGR>2.0.CO;2).
- Bruce, J., 1995: Eddies southwest of the Denmark Strait. *Deep-Sea Res. I*, **42**, 13–29, [https://doi.org/10.1016/0967-0637\(94\)00040-Y](https://doi.org/10.1016/0967-0637(94)00040-Y).
- Campin, J.-M., A. Adcroft, C. Hill, and J. Marshall, 2004: Conservation of properties in a free-surface model. *Ocean Modell.*, **6**, 221–244, [https://doi.org/10.1016/S1463-5003\(03\)00009-X](https://doi.org/10.1016/S1463-5003(03)00009-X).
- Cooper, L. H. N., 1955: Deep water movements in the North Atlantic as a link between climatic changes around Iceland and biological productivity of the English Channel and Celtic Sea. *J. Mar. Res.*, **14**, 347–362.
- Cummings, J. A., and O. M. Smedstad, 2013: Variational data assimilation for the global ocean. *Data Assimilation for Atmospheric, Oceanic and Hydrologic Applications*, S. Park and L. Xu, Eds., Vol. II, Springer, 303–343.
- Dee, D. P., and Coauthors, 2011: The ERA-Interim reanalysis: Configuration and performance of the data assimilation system. *Quart. J. Roy. Meteor. Soc.*, **137**, 553–597, <https://doi.org/10.1002/qj.828>.
- Dickson, B., and Coauthors, 2008: The overflow flux west of Iceland: Variability, origins and forcing. *Arctic–Subarctic Ocean Fluxes: Defining the Role of the Northern Seas in Climate*, R. R. Dickson, J. Meincke, and P. Rhines, Eds., Springer, 443–474, [https://doi.org/10.1007/978-1-4020-6774-7\\_20](https://doi.org/10.1007/978-1-4020-6774-7_20).
- Dickson, R. R., and J. Brown, 1994: The production of North Atlantic Deep Water: Sources, rates, and pathways. *J. Geophys. Res.*, **99**, 12 319–12 341, <https://doi.org/10.1029/94JC00530>.
- Donlon, C. J., M. Martin, J. Stark, J. Roberts-Jones, E. Fiedler, and W. Wimmer, 2012: The Operational Sea Surface Temperature and Sea Ice Analysis (OSTIA) system. *Remote Sens. Environ.*, **116**, 140–158, <https://doi.org/10.1016/j.rse.2010.10.017>.
- Eady, E. T., 1949: Long waves and cyclone waves. *Tellus*, **1** (3), 33–52, <https://doi.org/10.3402/tellusa.v1i3.8507>.
- Filyushkin, B. N., S. N. Moshonkin, S. A. Myslenkov, V. B. Zalesnyi, and N. G. Kozhelupova, 2013: Simulation of the interannual and seasonal variability of the overflow transport through the Denmark Strait. *Oceanology*, **53**, 643–654, <https://doi.org/10.1134/S0001437013050044>.
- Fischer, J., and Coauthors, 2015: Intra-seasonal variability of the DWBC in the western subpolar North Atlantic. *Prog. Oceanogr.*, **132**, 233–249, <https://doi.org/10.1016/j.pocean.2014.04.002>.
- Fristedt, T., R. Hietala, and P. Lundberg, 1999: Stability properties of a barotropic surface-water jet observed in the Denmark Strait. *Tellus*, **51A**, 979–989, <https://doi.org/10.3402/tellusa.v51i5.14506>.
- Gelderloos, R., T. W. N. Haine, I. M. Koszalka, and M. G. Magaldi, 2017: Seasonal variability in warm-water inflow toward Kangerdlugssuaq Fjord. *J. Phys. Oceanogr.*, **47**, 1685–1699, <https://doi.org/10.1175/JPO-D-16-0202.1>.
- Girton, J. B., and T. B. Sanford, 2003: Descent and modification of the overflow plume in the Denmark Strait. *J. Phys. Oceanogr.*, **33**, 1351–1364, [https://doi.org/10.1175/1520-0485\(2003\)033<1351:DAMOTO>2.0.CO;2](https://doi.org/10.1175/1520-0485(2003)033<1351:DAMOTO>2.0.CO;2).
- , —, and R. H. Käse, 2001: Synoptic sections of the Denmark Strait overflow. *Geophys. Res. Lett.*, **28**, 1619–1622, <https://doi.org/10.1029/2000GL011970>.
- Haine, T. W. N., 2010: High-frequency fluctuations in Denmark Strait transport. *Geophys. Res. Lett.*, **37**, L14601, <https://doi.org/10.1029/2010GL043272>.
- , S. Zhang, G. W. K. Moore, and I. A. Renfrew, 2009: On the impact of high-resolution, high-frequency meteorological



- forcing on Denmark Strait ocean circulation. *Quart. J. Roy. Meteor. Soc.*, **135**, 2067–2085, <https://doi.org/10.1002/qj.505>.
- Harden, B. E., R. S. Pickart, and I. A. Renfrew, 2014: Offshore transport of dense water from the east Greenland shelf. *J. Phys. Oceanogr.*, **44**, 229–245, <https://doi.org/10.1175/JPO-D-12-0218.1>.
- , and Coauthors, 2016: Upstream sources of the Denmark Strait overflow: Observations from a high-resolution mooring array. *Deep-Sea Res. I*, **112**, 94–112, <https://doi.org/10.1016/j.dsr.2016.02.007>.
- Harvey, J. G., 1961: Overflow of cold deep water across Iceland–Greenland Ridge. *Nature*, **189**, 911–913, <https://doi.org/10.1038/189911a0>.
- Helfrich, K. R., and L. J. Pratt, 2003: Rotating hydraulics and upstream basin circulation. *J. Phys. Oceanogr.*, **33**, 1651–1663, <https://doi.org/10.1175/2383.1>.
- Jackett, D. R., and T. J. McDougall, 1995: Minimal adjustment of hydrographic profiles to achieve static stability. *J. Atmos. Oceanic Technol.*, **12**, 381–389, [https://doi.org/10.1175/1520-0426\(1995\)012<0381:MAOHPT>2.0.CO;2](https://doi.org/10.1175/1520-0426(1995)012<0381:MAOHPT>2.0.CO;2).
- Jakobsson, M., and Coauthors, 2012: The International Bathymetric Chart of the Arctic Ocean (IBCAO) version 3.0. *Geophys. Res. Lett.*, **39**, L12609, <https://doi.org/10.1029/2012GL052219>.
- Jochumsen, K., D. Quadfasel, H. Valdimarsson, and S. Jónsson, 2012: Variability of the Denmark Strait overflow: Moored time series from 1996–2011. *J. Geophys. Res.*, **117**, C12003, <https://doi.org/10.1029/2012JC008244>.
- , M. Köllner, D. Quadfasel, S. Dye, B. Rudels, and H. Valdimarsson, 2015: On the origin and propagation of Denmark Strait overflow water anomalies in the Irminger Basin. *J. Geophys. Res. Oceans*, **120**, 1841–1855, <https://doi.org/10.1002/2014JC010397>.
- , M. Moritz, N. Nunes, D. Quadfasel, K. M. H. Larsen, B. Hansen, H. Valdimarsson, and S. Jónsson, 2017: Revised transport estimates of the Denmark Strait overflow. *J. Geophys. Res. Oceans*, **122**, 3434–3450, <https://doi.org/10.1002/2017JC012803>.
- Jónsson, S., 1999: The circulation in the northern part of the Denmark Strait and its variability. ICES Rep. CM-1999/L:06, 9 pp.
- , and H. Valdimarsson, 2004: A new path for the Denmark Strait overflow water from the Iceland Sea to Denmark Strait. *Geophys. Res. Lett.*, **31**, L03305, <https://doi.org/10.1029/2003GL019214>.
- , and —, 2012: Water mass transport variability to the North Icelandic shelf, 1994–2010. *ICES J. Mar. Sci.*, **69**, 809–815, <https://doi.org/10.1093/icesjms/fss024>.
- Junglaeus, J. H., A. Macrander, and R. H. Käse, 2008: Modelling the overflows across the Greenland–Scotland Ridge. *Arctic–Subarctic Ocean Fluxes: Defining the Role of the Northern Seas in Climate*, R. R. Dickson, J. Meincke, and P. Rhines, Eds., Springer, 527–549, [https://doi.org/10.1007/978-1-4020-6774-7\\_23](https://doi.org/10.1007/978-1-4020-6774-7_23).
- Käse, R. H., and A. Oschlies, 2000: Flow through Denmark Strait. *J. Geophys. Res.*, **105**, 28 527–28 546, <https://doi.org/10.1029/2000JC900111>.
- , J. B. Girtan, and T. B. Sanford, 2003: Structure and variability of the Denmark Strait overflow: Model and observations. *J. Geophys. Res.*, **108**, 3181, <https://doi.org/10.1029/2002JC001548>.
- Köhl, A., R. H. Käse, D. Stammer, and N. Serra, 2007: Causes of changes in the Denmark Strait overflow. *J. Phys. Oceanogr.*, **37**, 1678–1696, <https://doi.org/10.1175/JPO3080.1>.
- Kösters, F., R. H. Käse, A. Schmittner, and P. Herrmann, 2005: The effect of Denmark Strait overflow on the Atlantic meridional overturning circulation. *Geophys. Res. Lett.*, **32**, L04602, <https://doi.org/10.1029/2004GL022112>.
- Koszalka, I. M., T. W. N. Haine, and M. G. Magaldi, 2013: Fates and travel times of Denmark Strait Overflow Water in the Irminger Basin. *J. Phys. Oceanogr.*, **43**, 2611–2628, <https://doi.org/10.1175/JPO-D-13-023.1>.
- , —, and —, 2017: Mesoscale mixing of the Denmark Strait Overflow in the Irminger Basin. *Ocean Modell.*, **112**, 90–98, <https://doi.org/10.1016/j.ocemod.2017.03.001>.
- Large, W. G., J. C. McWilliams, and S. C. Doney, 1994: Oceanic vertical mixing: A review and a model with a nonlocal boundary layer parameterization. *Rev. Geophys.*, **32**, 363–403, <https://doi.org/10.1029/94RG01872>.
- Lea, D. J., T. W. N. Haine, and R. F. Gasparovic, 2006: Observability of the Irminger Sea circulation using variational data assimilation. *Quart. J. Roy. Meteor. Soc.*, **132**, 1545–1576, <https://doi.org/10.1256/qj.05.77>.
- Logemann, K., J. Ólafsson, A. Snorrason, H. Valdimarsson, and G. Marteinsdóttir, 2013: The circulation of Icelandic waters—A modelling study. *Ocean Sci.*, **9**, 931–955, <https://doi.org/10.5194/os-9-931-2013>.
- Losch, M., D. Menemenlis, J.-M. Campin, P. Heimbach, and C. Hill, 2010: On the formulation of sea-ice models. Part 1: Effects of different solver implementations and parameterizations. *Ocean Modell.*, **33**, 129–144, <https://doi.org/10.1016/j.ocemod.2009.12.008>.
- Macrander, A., U. Send, H. Valdimarsson, S. Jónsson, and R. H. Käse, 2005: Interannual changes in the overflow from the Nordic Seas into the Atlantic Ocean through Denmark Strait. *Geophys. Res. Lett.*, **32**, L06606, <https://doi.org/10.1029/2004GL021463>.
- , R. H. Käse, U. Send, H. Valdimarsson, and S. Jónsson, 2007: Spatial and temporal structure of the Denmark Strait overflow revealed by acoustic observations. *Ocean Dyn.*, **57**, 75–89, <https://doi.org/10.1007/s10236-007-0101-x>.
- Magaldi, M. G., and T. W. N. Haine, 2015: Hydrostatic and non-hydrostatic simulations of dense waters cascading off a shelf: The east Greenland case. *Deep-Sea Res. I*, **96**, 89–104, <https://doi.org/10.1016/j.dsr.2014.10.008>.
- , —, and R. S. Pickart, 2011: On the nature and variability of the East Greenland Spill Jet: A case study in summer 2003. *J. Phys. Oceanogr.*, **41**, 2307–2327, <https://doi.org/10.1175/JPO-D-10-05004.1>.
- Marshall, J., A. Adcroft, C. Hill, L. Perelman, and C. Heisey, 1997: A finite-volume, incompressible Navier Stokes model for studies of the ocean on parallel computers. *J. Geophys. Res.*, **102**, 5753–5766, <https://doi.org/10.1029/96JC02775>.
- Mastropole, D., R. S. Pickart, H. Valdimarsson, K. Våge, K. Jochumsen, and J. Girtan, 2017: On the hydrography of Denmark Strait. *J. Geophys. Res. Oceans*, **122**, 306–321, <https://doi.org/10.1002/2016JC012007>.
- Medvedev, D., G. Lemson, and M. Rippin, 2016: SciServer compute: Bringing analysis close to the data. *Proc. 28th Int. Conf. on Scientific and Statistical Database Management*, New York, NY, Association for Computing Machinery, 27, <https://doi.org/10.1145/2949689.2949700>.
- Nikolopoulos, A., K. Borenäs, R. Hietala, and P. Lundberg, 2003: Hydraulic estimates of Denmark Strait overflow. *J. Geophys. Res.*, **108**, 3095, <https://doi.org/10.1029/2001JC001283>.
- Noël, B., W. J. van de Berg, H. Machguth, S. Lhermitte, I. Howat, X. Fettweis, and M. R. van den Broeke, 2016: A daily, 1 km resolution data set of downscaled Greenland Ice Sheet surface mass balance (1958–2015). *Cryosphere*, **10**, 2361–2377, <https://doi.org/10.5194/tc-10-2361-2016>.

- Pedlosky, J., 1979: *Geophysical Fluid Dynamics*. Springer-Verlag, 624 pp.
- Resdler, R., and C. W. Böning, 1997: Effect of the overflows on the circulation in the subpolar North Atlantic: A regional model study. *J. Geophys. Res.*, **102**, 18 529–18 552, <https://doi.org/10.1029/97JC00021>.
- Reszka, M. K., G. E. Swaters, and B. R. Sutherland, 2002: Instability of abyssal currents in a continuously stratified ocean with bottom topography. *J. Phys. Oceanogr.*, **32**, 3528–3550, [https://doi.org/10.1175/1520-0485\(2002\)032<3528:IOACIA>2.0.CO;2](https://doi.org/10.1175/1520-0485(2002)032<3528:IOACIA>2.0.CO;2).
- Ross, C., 1984: Temperature–salinity characteristics of the “overflow” water in Denmark Strait during “OVERFLOW ’73.” *Rapports et Procès-Verbaux des Réunions Conseil International pour l’Exploration de la Mer* **185**, 111–119.
- Rudels, B., P. Eriksson, H. Grönvall, R. Hietala, and J. Launiainen, 1999: Hydrographic observations in Denmark Strait in fall 1997, and their implications for the entrainment into the overflow plume. *Geophys. Res. Lett.*, **26**, 1325–1328, <https://doi.org/10.1029/1999GL900212>.
- , E. Fahrbach, J. Meincke, G. Budus, and P. Eriksson, 2002: The East Greenland Current and its contribution to the Denmark Strait overflow. *ICES J. Mar. Sci.*, **59**, 1133–1154, <https://doi.org/10.1006/jmsc.2002.1284>.
- Sakov, P., F. Counillon, L. Bertino, K. A. Lisæter, P. R. Oke, and A. Korabev, 2012: TOPAZ4: An ocean-sea ice data assimilation system for the North Atlantic and Arctic. *Ocean Sci.*, **8**, 633–656, <https://doi.org/10.5194/os-8-633-2012>.
- Schweckendiek, U., and J. Willebrand, 2005: Mechanisms affecting the overturning response in global warming simulations. *J. Climate*, **18**, 4925–4936, <https://doi.org/10.1175/JCLI3550.1>.
- Smith, P. C., 1976: Baroclinic instability in the Denmark Strait overflow. *J. Phys. Oceanogr.*, **6**, 355–371, [https://doi.org/10.1175/1520-0485\(1976\)006<0355:BIITDS>2.0.CO;2](https://doi.org/10.1175/1520-0485(1976)006<0355:BIITDS>2.0.CO;2).
- Smith, W. H. F., and D. T. Sandwell, 1997: Global sea floor topography from satellite altimetry and ship depth soundings. *Science*, **277**, 1956–1962, <https://doi.org/10.1126/science.277.5334.1956>.
- Spall, M. A., and J. F. Price, 1998: Mesoscale variability in Denmark Strait: The PV outflow hypothesis. *J. Phys. Oceanogr.*, **28**, 1598–1623, [https://doi.org/10.1175/1520-0485\(1998\)028<1598:MVIDST>2.0.CO;2](https://doi.org/10.1175/1520-0485(1998)028<1598:MVIDST>2.0.CO;2).
- Strass, V. H., E. Fahrbach, U. Schauer, and L. Sellmann, 1993: Formation of Denmark Strait Overflow Water by mixing in the East Greenland Current. *J. Geophys. Res.*, **98**, 6907–6919, <https://doi.org/10.1029/92JC02732>.
- Sutherland, D. A., F. Straneo, G. B. Stenson, F. J. Davidson, M. O. Hammill, and A. Rosing-Asvid, 2013: Atlantic water variability on the SE Greenland continental shelf and its relationship to SST and bathymetry. *J. Geophys. Res. Oceans*, **118**, 847–855, <https://doi.org/10.1029/2012JC008354>.
- Swaters, G. E., 1991: On the baroclinic instability of cold-core coupled density fronts on a sloping continental shelf. *J. Fluid Mech.*, **224**, 361–382, <https://doi.org/10.1017/S0022112091001799>.
- Våge, K., R. S. Pickart, M. A. Spall, H. Valdimarsson, S. Jónsson, D. J. Torres, S. Østerhus, and T. Eldevik, 2011: Significant role of the north Icelandic jet in the formation of Denmark Strait Overflow Water. *Nat. Geosci.*, **4**, 723–727, <https://doi.org/10.1038/ngeo1234>.
- , —, —, G. Moore, H. Valdimarsson, D. J. Torres, S. Y. Erofeeva, and J. E. Nilsen, 2013: Revised circulation scheme north of the Denmark Strait. *Deep-Sea Res. I*, **79**, 20–39, <https://doi.org/10.1016/j.dsr.2013.05.007>.
- Vallis, G. K., 2006: *Atmospheric and Oceanic Fluid Dynamics*. Cambridge University Press, 745 pp.
- von Appen, W.-J., R. S. Pickart, K. H. Brink, and T. W. Haine, 2014a: Water column structure and statistics of Denmark Strait Overflow Water cyclones. *Deep-Sea Res. I*, **84**, 110–126, <https://doi.org/10.1016/j.dsr.2013.10.007>.
- , and Coauthors, 2014b: The East Greenland Spill Jet as an important component of the Atlantic meridional overturning circulation. *Deep-Sea Res. I*, **92**, 75–84, <https://doi.org/10.1016/j.dsr.2014.06.002>.
- , D. Mastropole, R. S. Pickart, H. Valdimarsson, S. Jónsson, and J. B. Girtton, 2017: On the nature of the mesoscale variability in Denmark Strait. *J. Phys. Oceanogr.*, **47**, 567–582, <https://doi.org/10.1175/JPO-D-16-0127.1>.
- Whitehead, J. A., 1998: Topographic control of oceanic flows in deep passages and straits. *Rev. Geophys.*, **36**, 423–440, <https://doi.org/10.1029/98RG01014>.
- , A. Leetmaa, and R. A. Knox, 1974: Rotating hydraulics of strait and sill flows. *Geophys. Fluid Dyn.*, **6**, 101–125, <https://doi.org/10.1080/03091927409365790>.